

IMPROVEMENT OF THE SPATIAL RESOLUTION OF THE ACIS USING SPLIT-PIXEL EVENTS

HIROSHI TSUNEMI,^{1,2} KOJI MORI,^{1,3} EMI MIYATA,^{1,2} CHRISTOPHER BALUTA,¹ DAVID N. BURROWS,³
GORDON P. GARMIRE,³ AND GEORGE CHARTAS³

Received 2000 December 19; accepted 2001 February 6

ABSTRACT

The position accuracy of X-ray photons on a CCD detector is generally believed to be limited by the CCD pixel size. While this is true in general, the position accuracy for X-ray events which deposit charge in more than one pixel can be better than that of the CCD pixel size. Since the position uncertainty for corner events is much better than the pixel size, we can improve the *Chandra* ACIS spatial resolution by selecting only these events. We have analyzed X-ray images obtained with the *Chandra* ACIS for six pointlike sources observed near the optical axis. The image quality near the optical axis is characterized by a half-power diameter (HPD) of 0".66 that is a convolution of the point-spread function (PSF) of the high-resolution mirror assembly (HRMA) and the CCD pixel shape (24 μm square). By considering only corner events the image quality is improved to 0".56 (HPD) at the optical axis, which is very close to the image quality of the HRMA alone. We estimated the degradation of the image quality obtained by using all events, compared to that obtained using only corner events, to be 0".33, which coincides with that expected from the pixel size. Since the fraction of the corner events is relatively small, this technique requires correspondingly longer exposure time to achieve good statistics.

Subject headings: instrumentation: detectors — methods: data analysis —
techniques: image processing — X-rays: general

1. INTRODUCTION

Chandra X-Ray Observatory is the first X-ray imaging satellite to have an image quality that is comparable to that of optical images. The point-spread function (PSF) of the high-resolution mirror assembly (HRMA) has a half-power diameter (HPD) of about one-half arcsecond (*Chandra* Proposers' Observatory Guide 2000⁴), which corresponds to 24 μm on the focal plane. The detector system should oversample the PSF in order to achieve the highest imaging capability. *Chandra* has two types of nondispersive detector systems: the Advanced CCD Imaging Spectrometer (ACIS), a CCD array, and the high-resolution camera (HRC), a microchannel plate. The CCD chip employed in the ACIS is a frame transfer device with 24 μm square pixels (Burke et al. 1997) and moderate energy resolution. The overall PSF of the *Chandra*/ACIS image is a convolution of the PSF of the HRMA and the pixel shape of the CCD. Because the pixel size of the CCD is comparable to the HPD of the HRMA, the image quality is somewhat degraded. The HRC has higher spatial resolution ($\sim 20 \mu\text{m}$ FWHM, with 6.4 μm pixels), but with poor energy resolution. The observer therefore needs to choose the detector system depending on the required combination of angular resolution and energy resolution.

Because the CCD pixel boundaries are sharply delineated by physical structures on the detector, we can utilize the morphology of X-ray events that split charge between pixels to provide detector position information on a size scale

much smaller than the actual pixel size. In § 2, we explain the process of charge generation and division within the CCD pixel. In § 3, we describe our method for subpixel resolution. In § 4, we apply this method to *Chandra*/ACIS data for six point sources and show that the method does indeed recover the inherent angular resolution of the HRMA, although at the price of reduced observing efficiency.

2. X-RAY DETECTION IN A CCD

The process of detection of X-rays in a CCD has been discussed in detail by Lumb & Nousek (1993) and by L. K. Townsley et al. (2001, in preparation). Here we provide an abbreviated discussion of these processes sufficient to explain our method for subpixel resolution. A CCD is ordinarily used in photon-counting mode to detect X-rays. To make this possible, the count rate must be low enough (and the exposure short enough) that at most one photon is detected per frame in any given 3×3 "neighborhood" of pixels. When an X-ray photon enters the CCD, it is captured by photoelectric absorption and generates a primary charge cloud in which the number of electrons is proportional to the incident X-ray energy. An X-ray photon of 1 keV, for example, generates about 275 electrons, while an optical photon generates only one or two electrons. Figure 1 schematically shows the evolution of a primary charge cloud generated by X-ray photons inside the CCD. The primary charge cloud expands through diffusion as it travels through the depletion region of the CCD to the buried channel, where the charge is collected into pixel structures defined by electric fields near the surface of the CCD. Before being captured into the photon entrance pixel, the primary charge cloud generated by an X-ray photon absorbed near the back of the depletion region can spread into neighboring pixels, creating a "split-pixel event." By contrast, an X-ray photon absorbed in or near the buried channel will typically deposit its charge in a single pixel, and

¹ Department of Earth and Space Science, Graduate School of Science, Osaka University, 1-1 Machikaneyama, Toyonaka, Osaka 560-0043, Japan; tsunemi@ess.sci.osaka-u.ac.jp, mori@ess.sci.osaka-u.ac.jp, miyata@ess.sci.osaka-u.ac.jp, baluta@ess.sci.osaka-u.ac.jp.

² CREST, Japan Science and Technology Corporation (JST).

³ Department of Astronomy and Astrophysics, 525 Davey Laboratory, Penn State University, University Park, PA 16802; burrows@astro.psu.edu, garmire@acis.astro.psu.edu, chartas@lonestar.astro.psu.edu.

⁴ See <http://asc.harvard.edu/udocs/udocs/POG/MPOG/>.

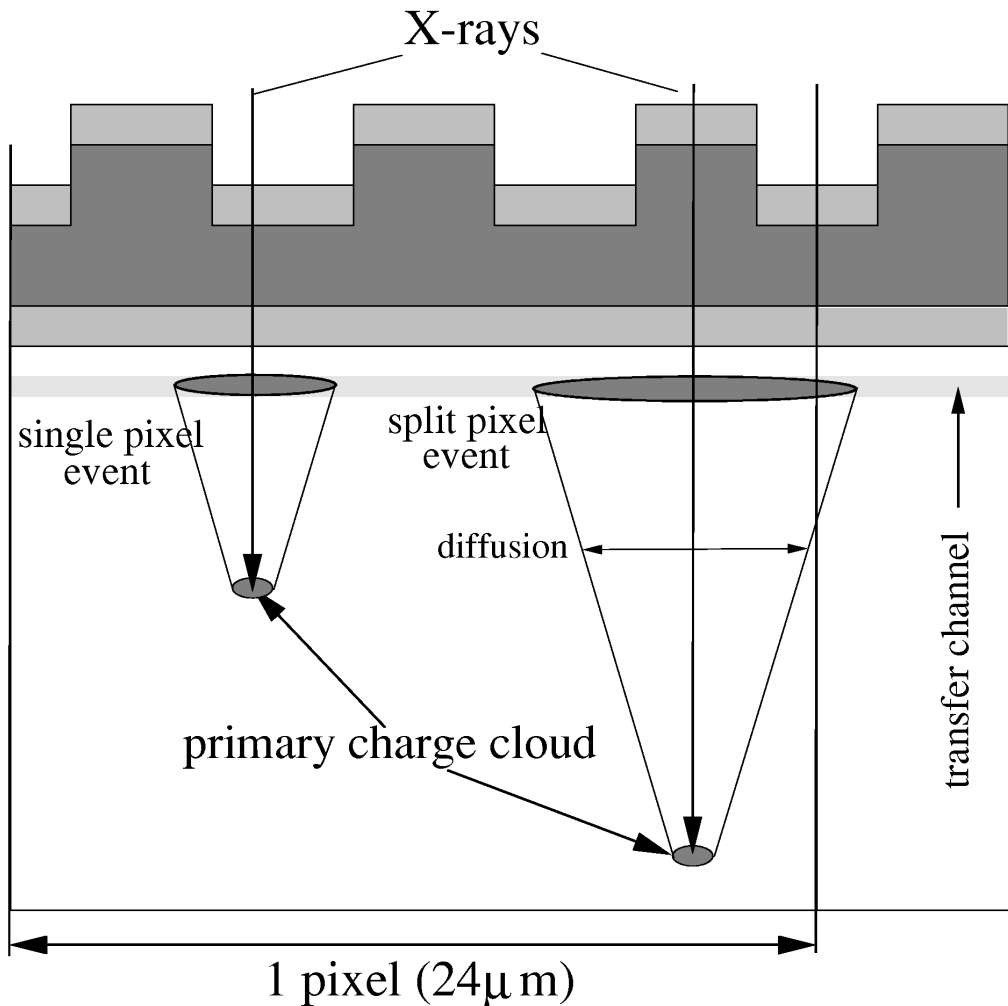


FIG. 1.—Schematic view of the evolution of a primary charge cloud generated by X-ray photons inside a front-illuminated CCD

the resulting charge packet is referred to as a “single-pixel event.” The incident X-ray energy is estimated by summing up the signal contained inside the event. Because the output from each pixel contains noise, single-pixel events usually have a better energy resolution than do split-pixel events.

The size of the primary charge cloud depends on the travel distance in the depletion layer and the electric field inside the CCD. If the CCD is front illuminated (FI), the travel distance in the depletion region depends on where the photoabsorption occurs and therefore depends strongly on the photon energy. The shorter the attenuation length for an X-ray photon, the smaller the primary charge cloud will be. The X-ray photons used in our analysis are mainly around 1 keV (near the peak effective area of the instrument) and have a relatively short attenuation length in silicon compared with the depletion depth or the pixel size of the CCD. Therefore, they are photoabsorbed in a relatively shallow region of the depletion layer. On the contrary, if the CCD is back illuminated (BI), a 1 keV photon is absorbed near the back surface; the travel distance will be the depth of the depletion layer and is almost independent of the X-ray energy. Applying a simple diffusion model, the primary charge cloud size will be a few microns for the BI CCD and smaller for the FI CCD. This explains qualitatively why objects observed with the FI CCD show a higher

fraction of single-pixel events in the branching ratio than those observed with the BI CCD.

The spreading of the charge cloud is less than typical CCD pixel sizes, and X-ray events may contain charge in more than one adjacent pixel in excess of the local bias level and/or dark current, with most true X-ray events (as opposed to particle-induced background events) containing no more than four adjacent pixels. X-ray events are classified by their morphology, with two common systems being the eight grades used by *ASCA* (grades 0–7) and the 256 grades used by the ACIS instrument (fitgrades 0–255). Further details regarding *ASCA* grades are given in Yamashita et al. (1997) while § 6.4 of the *Chandra* Proposers’ Observatory Guide (2000)⁵ describes ACIS fitgrade.

3. SUBPIXEL RESOLUTION METHOD FOR *CHANDRA*/ACIS

Because the primary charge cloud generated inside the CCD expands through diffusion, the position on the CCD where the X-ray entered can be precisely determined if the center of gravity of this charge cloud can be measured. If the

⁵ See <http://asc.harvard.edu/udocs/udocs/POG/MPOG/>.

primary charge cloud remains within a single pixel (a single-pixel event), its centroid cannot be determined, and one generally assumes that the X-ray photon landed in the center of that pixel, with an uncertainty of about one-half of a pixel. However, if an X-ray photon is absorbed near a pixel boundary, the primary charge cloud splits into the adjacent pixel(s), forming a split-pixel event, and the centroid of the charge distribution can be used to precisely locate, in at least one dimension, the position at which the photon was absorbed. The charge cloud size determines the size of the boundary region within which the X-ray photon becomes a split event. The pixel is therefore divided into three classes of regions that characterize single-pixel events (from the center of the pixel), two-pixel split events (from the pixel edges), and three- or four-pixel split events (from the pixel corners). The ratios among the areas for these three regions can be roughly estimated from the branching ratio of these X-ray event grades.

This technique has been verified by our mesh experiments (Tsunemi, Yoshita, & Kitamoto 1997; Tsunemi et al. 1998). In these experiments, we placed a metal mesh with many small periodically spaced holes just above the CCD. Such a setup enables us to directly measure the primary charge cloud shape (Hiraga et al. 1998). We thus found that the charge cloud shape is well expressed by a Gaussian function with a standard deviation (σ) for 1–4 keV photons of about 1–2 μm (Tsunemi et al. 1999). Although the charge cloud shape depends on the CCD chip, the charge cloud size for an X-ray photon with energy of a few keV is at most a few microns. Knowledge of the grade of an event, combined with the relatively narrow size of the charge cloud, allows the position at which the X-ray enters the CCD to be determined with subpixel resolution (Hiraga, Tsunemi, & Miyata 2001).

Based on these results, we can safely estimate the primary charge cloud size generated by an X-ray photons with energy of a few keV inside the ACIS CCD chip to be a few microns. The mesh experiment applied to the ACIS CCD shows that split events are generated very near to the pixel boundary (Pivovarov et al. 1998). The grade information of the X-ray event will thus specify the entering position within the pixel to high accuracy for X-rays absorbed near the pixel boundaries. For single-pixel events, the photon can only be localized to a region slightly smaller than the pixel size. The two-pixel split events can be identified only with a pixel edge, which provides high resolution in one dimension. The greatest improvement for the X-ray position resolution is achieved for three- or four-pixel split events (corner events), which are generated when the X-ray enters the CCD very close to a pixel corner. The X-ray entering position must be within one charge cloud size from the pixel corner. This allows us to improve on the spatial resolution of the pixel size by roughly a factor of 10, based solely on the event grade.

This is of practical use for data obtained by *Chandra* because, unlike the *HST*, which points very accurately at a fixed position during observations, *Chandra* is intentionally moved slowly across the sky during each observation. This “dithering” motion of the observatory moves the target image across the CCD surface, forming a Lissajous figure with an amplitude of about 20 pixels and a period of about 1000 s. Therefore, X-rays from a point source do not always enter the same subpixel position of the same pixel, but have randomly distributed subpixel positions. Some photons

enter the central part of the pixel, forming single-pixel events, while others enter the pixel boundary, forming split-pixel events. The latter can be used to achieve higher spatial resolution than that determined by the pixel size. Strictly speaking, the image shape can vary according to the dithering motion. With taking into account the amplitude of the dithering motion, the degradation of the image quality concerned is negligibly small compared to the actual PSF of the HRMA.

The method we employ is quite simple. First, we discard all X-ray events except for corner events (ACIS fltgrades 10, 11, 18, 22, 72, 80, 104, and 208). We know that these remaining events entered the detector near a pixel corner but were projected onto the sky as if they had entered at the pixel center. We therefore need to shift the sky coordinates for these events by one-half of a pixel along each axis in detector coordinates. To do this, we need to know the orientation of the CCD chip projected onto the sky coordinates. This is given by the roll angle of the spacecraft, which is specified in the header keyword of the event file. We then can shift the position for corner events by half the pixel size (which is 0'246) along both pixel sides. The actual shift direction depends on the CCD chip employed and the roll angle as well as the fltgrade of the event. The resulting sky positions accurately reflect the actual incident positions on the CCD detector to within about 0'05 for perfect attitude knowledge.

4. RESULTS

To test this method, we searched our GTO data and publicly available calibration data for pointlike sources with appropriate characteristics. We selected sources with good statistics (at least 1500 total counts) and that are close to the optical axis (within 75") in order to avoid possible distortion. We selected six pointlike sources: two stars and four AGNs. The two stars, which we refer to as “source 1” ($5^{\text{h}}35^{\text{m}}15^{\text{s}}.67$, $-5^{\circ}23'11''.2$) and “source 2” ($5^{\text{h}}35^{\text{m}}15^{\text{s}}.73$, $-5^{\circ}23'15''.5$), are in the Orion Nebula. Two AGNs, PKS 0312–770 and PG 1634+706, come from the public data. The other source contains the two gravitationally lensed images of the quasar Q0957+561, named “image A” and “image B” (Walsh, Carswell, & Weymann 1979). Three sources are observed with the FI CCD while the others are observed with the BI CCD.

We removed the subpixel randomization usually applied in the standard data processing at the *Chandra X-Ray Center* so that we can assess the precise X-ray entering position on the detector. Townsley et al. (2000) developed a charge transfer inefficiency (CTI) correction method that could correct the “grade migration” (the corruption of event grades caused by poor charge transfer efficiency in the FI CCDs) for the data obtained after 1999 September 16. We applied their method to five data sets out of six, since it could not cover the data for PKS 0312–770. The observational configurations are summarized in Table 1.

We then sorted all the X-ray events (all events) according to the event geometry on the CCD. Specifically, they were sorted as single-pixel events, two-pixel split events, and corner events. Furthermore, they were sorted according to the event geometry within the 3×3 pixels using the “fltgrade” (see the *Chandra* Proposers' Observatory Guide). In this way, we sorted the event list into nine groups: one single-pixel event group, four two-pixel split event groups, and four corner-event groups. The statistics

TABLE 1
SUMMARY OF THE OBSERVATIONS

PROPERTY	ORION NEBULA				Q0957+561		
	Source 1	Source 2	PG 1634+706	PKS 0312-770	Image B	Image A	
Obs ID	18	18	69	1109	362	362	
Category	Star	Star	AGN	AGN	AGN	AGN	
CCD chip	FI	FI	BI	FI	BI	BI	
Exposure (ks)	46.94	46.94	4.80	13.00	47.26	47.26	
Distance (arcsec) ^a	6.9	11.	19	20	69	72	
CTI correction	Yes	Yes	Yes	No	Yes	Yes	
Event Grade	fltgrade		Number of Events				
Single pixel	0	5663	5132	607	1321	4303	5763
Two-pixel split:							
Down	2	364	279	241	238	1135	1478
Left	8	683	383	198	199	1084	1429
Right	16	685	348	232	188	1078	1408
Up	64	864	531	223	393	1125	1469
Corner:							
Left-down	10,11	220	72	83	70	328	475
Right-down	18,22	227	65	65	74	329	456
Left-up	72,104	202	82	58	104	305	392
Right-up	80,208	215	67	73	96	308	474

^a Angular distance from the optical axis in arcseconds.

for each grade are summarized in Table 1. We then extracted the images in absolute sky coordinates, which places each event on the sky at the projection of the central pixel of the 3 × 3 pixel event neighborhood.

Figure 2 shows an example of the distributions of four groups of corner events for Q0957+561 image A in absolute sky coordinates that is obtained by employing uncor-

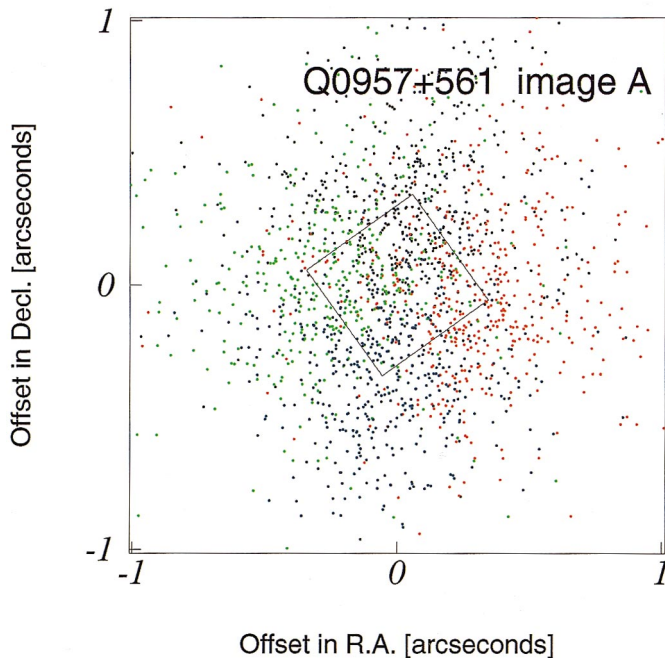


FIG. 2.—Plot of the distribution of corner events for Q0957+561 vs. absolute sky coordinates. The four groups, left-down (black), right-down (red), left-up (green), and right-up (blue), are clearly separated from each other. The square represents the ACIS pixel in its proper orientation.

rected events. One can clearly see the systematic shift of their centers of gravity, depending on the fltgrade of the event. Figure 3 shows the centers of gravity for all nine event types discussed here in absolute sky coordinates for six sources, where the square shows the pixel shape projected on the sky with the proper orientation. These figures are also obtained by using uncorrected events. We confirm that the distribution of the single-pixel events coincides with the nominal position, which is the center of the central pixel of the event. As expected, the centers of gravity of the two-pixel events lie near the centers of the pixel edges, while the centers of gravity of the three- and four-pixel events fall near the pixel corners. Because the software places these uncorrected events at the centers of the pixels instead of at their true corner locations, they end up at incorrect celestial locations, with the centroids of the four corner-event groups making an inverted image of the pixel. Applying the correction discussed in this paper would make the four-pixel clouds lie on top of one another.

Figure 4 shows images obtained using corrected corner events, as well as those obtained from all events for comparison. Since we find that all images are almost point symmetric, we fit them with a point-symmetric Gaussian function with constant background. The background is less than 1% of the count rate of the source. We then calculated the HPD from the best fit Gaussian function for each image. The results are summarized in Table 2 where all errors are 90% confidence levels. HPD_{all} and HPD_c represent the HPDs for the images for all events and for the corner events, respectively.

The actual HPD can be easily measured by counting the number of events. In this measurement, we assume the center of the Gaussian function determines the image center. We then count the number of events contained in a circle as a function of diameter. We define the actual HPD

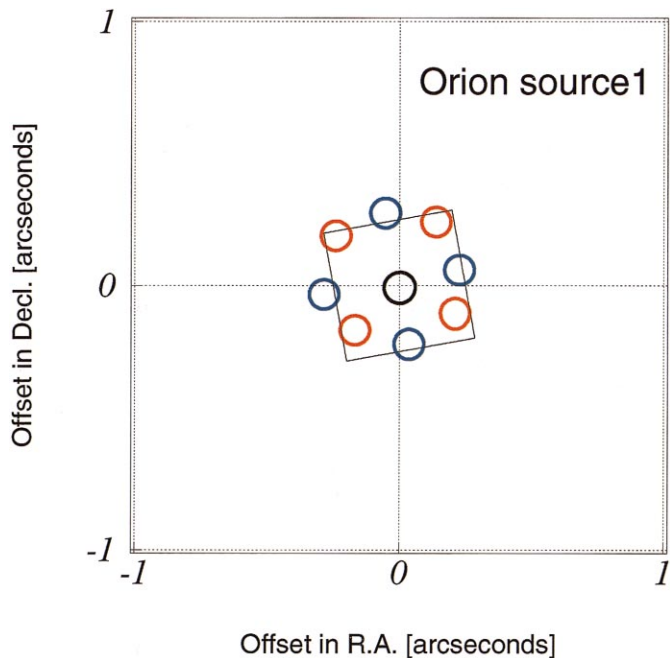


FIG. 3a

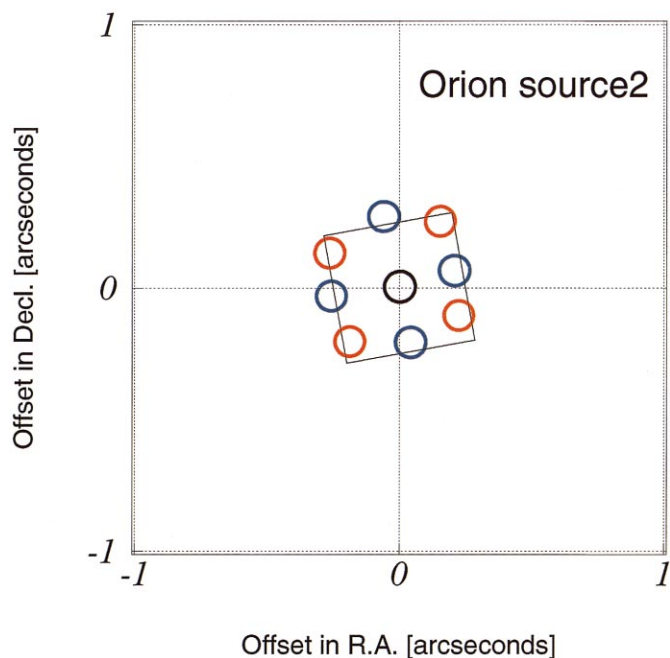


FIG. 3b

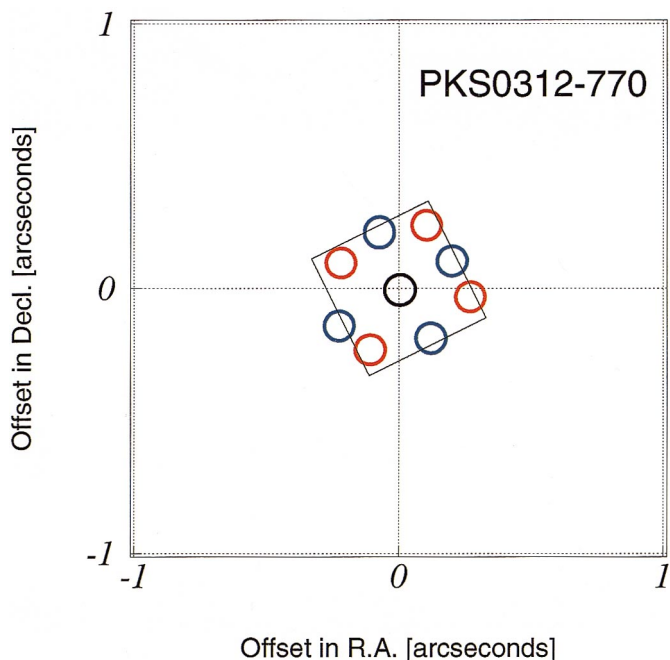


FIG. 3c

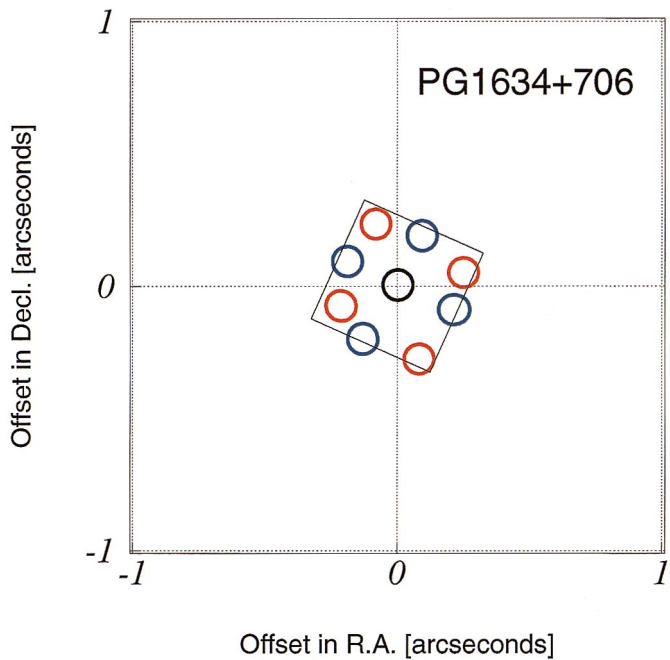


FIG. 3d

FIG. 3.—Plot of the distribution of the centers of gravity for corner events (*red*), two-pixel split events (*blue*), and single-pixel events (*black*) vs. the absolute sky coordinates for the Orion Nebula (*a*) source 1, (*b*) source 2, (*c*) PKS 0312 – 770, (*d*) PG 1634 + 706, and Q0957 + 561 (*e*) image A, and (*f*) image B. The uncertainties for the centers of gravity are comparable to or smaller than these marks. The square shows a pixel shape in its proper orientation.

as the diameter of the circle that contains half of the events appeared in a circle of $4''$ in diameter. We confirmed that the actual HPD measured are consistent with those obtained by fitting the Gaussian function within statistical uncertainties.

5. DISCUSSION

The PSF of the HRMA has a size of about $0''.5$ HPD on the optical axis, which corresponds to about $24 \mu\text{m}$ on the detector. The HPD of the final image is the root mean square of that for the HRMA and that for the CCD pixel.

The σ for a square distribution is $(a^2/12)^{1/2}$ where “ a ” is the square size. If we use $2(2\ln 2)^{1/2}$ as the conversion factor from σ to HPD just as the case of the Gaussian function, the HPD for the ACIS CCD pixel is about $16 \mu\text{m}$, which is the HPD for all events if the subpixel position of the photon is unknown.

Therefore, the HPD of the final image obtained for all events will be $29 \mu\text{m}$ on the detector or $0''.59$ when projected onto the sky. However, the position accuracy of the corner events is about a few microns since their distribution is within the charge cloud shape. This value is negligibly small

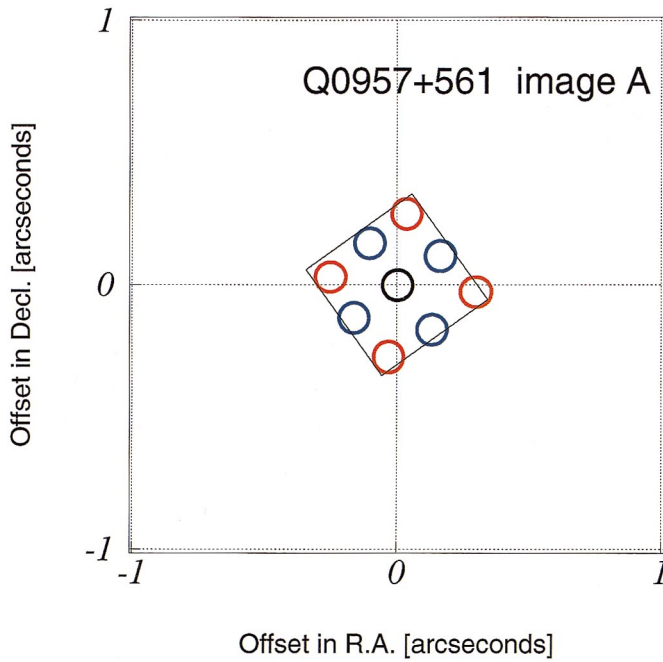


FIG. 3e

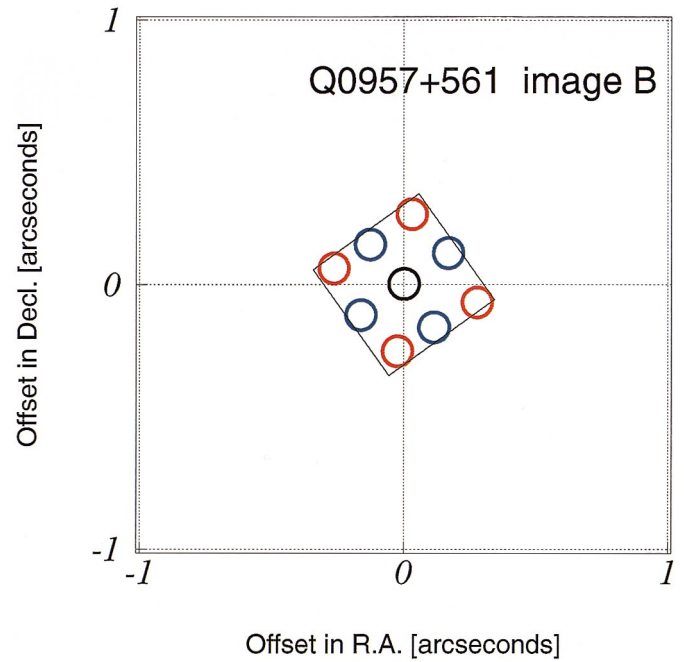


FIG. 3f

compared with the PSF of the HRMA and does not degrade it.

We can estimate the improvement of the position resolution between all events and the corner events by $\Delta\text{HPD} = (\text{HPD}_{\text{all}}^2 - \text{HPD}_c^2)^{1/2}$, as listed in Table 2. Figure 5 shows a plot of ΔHPD along the angular distance from the optical axis as well as HPD_{all} and HPD_c . We found $\Delta\text{HPD} = 0''.35 \pm 0''.07$ by using all the data. This corresponds to $17 \pm 3 \mu\text{m}$ on the detector. This shows that by using only corner events we can significantly reduce the PSF degradation caused by the undersampling of the PSF by the ACIS pixels. Practically, we can say that the image degradation by all events is noticeable while that by the corner events is negligibly small.

In principle, the effective resolution could be improved further by using both the knowledge of the charge cloud shape and that of the grade of the multipixel events to determine the exact position of the X-ray within the boundary region. Actually the primary charge cloud shape is known as the position on the CCD where the X-ray entered can be determined for split-pixel events with submicron resolution (Hiraga et al. 2001). The simplifying assumption that we have made here is that, even if the charge cloud shape is not known, we can assume that the X-ray entering position for corner events is precisely at the pixel corner. For *Chandra*, the angular uncertainty associated with this assumption is much smaller than the PSF of the HRMA.

These data demonstrate that the boundary region itself is sufficiently small that this additional information would not significantly improve the PSF.

The fraction of the corner events, which depends on the incident X-ray spectrum as well as on the CCD type, is about 4%–16% of the total events. Thus, this technique, while able to improve the effective angular resolution of *Chandra*, does so at the cost of low efficiency. However, we have shown that this technique is effective, even for as few as 300 corner events.

6. CONCLUSION

We have demonstrated that X-ray split events on the CCD can yield position information more precise than the pixel size. The *Chandra Observatory* has a dither motion that moves the target on the detector so that the X-rays are absorbed uniformly over the pixels. Therefore, some fraction of the X-ray photons always generate corner events that can be used to achieve the finer image without degradation by the CCD pixel size.

We have studied six pointlike sources that were observed near the optical axis. Since the split events are generated near the CCD pixel boundary, we can determine the X-ray entering position with much better resolution than the pixel size. The average image size using the corner events is $0''.56$ (HPD) at the optical axis while that using all events is

TABLE 2
IMAGE SIZE (HPD [ARCSEC])

TARGET	ORION NEBULA		Q0957 + 561			
	Source 1	Source 2	PG 1634 + 706	PKS 0312 – 770	Image B	Image A
HPD _c	0.52 ± 0.02	0.60 ± 0.04	0.61 ± 0.04	0.49 ± 0.02	0.67 ± 0.02	0.67 ± 0.02
HPD _{all}	0.64 ± 0.01	0.71 ± 0.01	0.69 ± 0.02	0.65 ± 0.02	0.74 ± 0.01	0.75 ± 0.01
ΔHPD^a	0.37 ± 0.03	0.37 ± 0.06	0.32 ± 0.09	0.43 ± 0.04	0.33 ± 0.05	0.33 ± 0.04

NOTE—Errors quoted are 90% confidence levels.

^a $\Delta\text{HPD} = (\text{HPD}_{\text{all}}^2 - \text{HPD}_c^2)^{1/2}$.

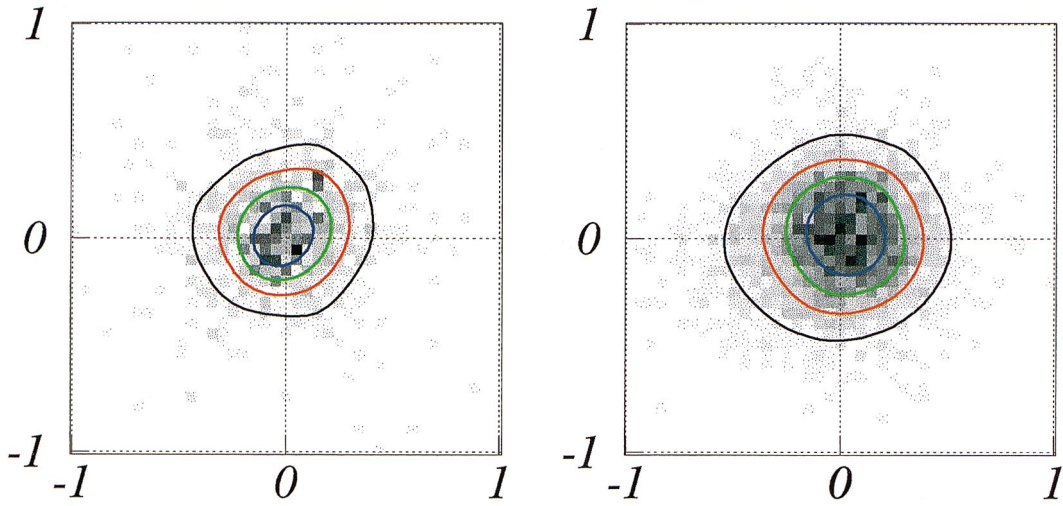


FIG. 4a

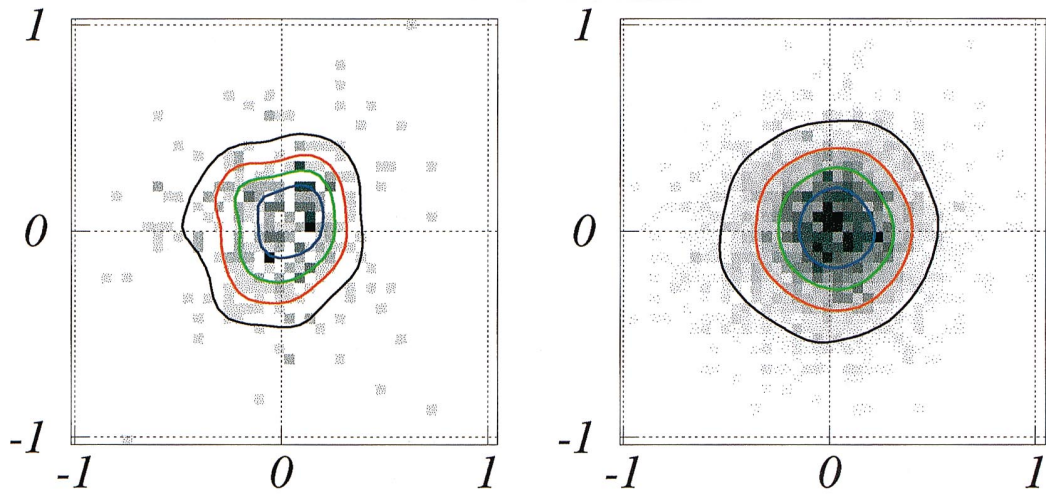


FIG. 4b

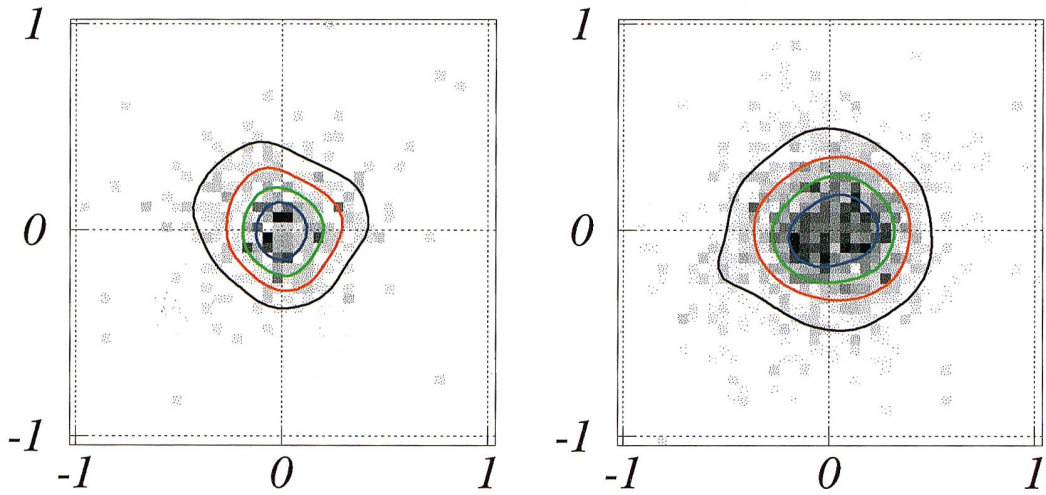


FIG. 4c

FIG. 4.—X-ray images for six sources: the Orion Nebula (a) source 1, (b) source 2, (c) PKS 0312 – 770, (d) PG 1634 + 706, and Q0957 + 561 (e) image A, and (f) image B. The left side of each figure is the image obtained with corner events shifted by half-pixel size while the right side is obtained with all events. Contour levels are on a linear scale, showing 20%, 40%, 60%, and 80% of the peak value.

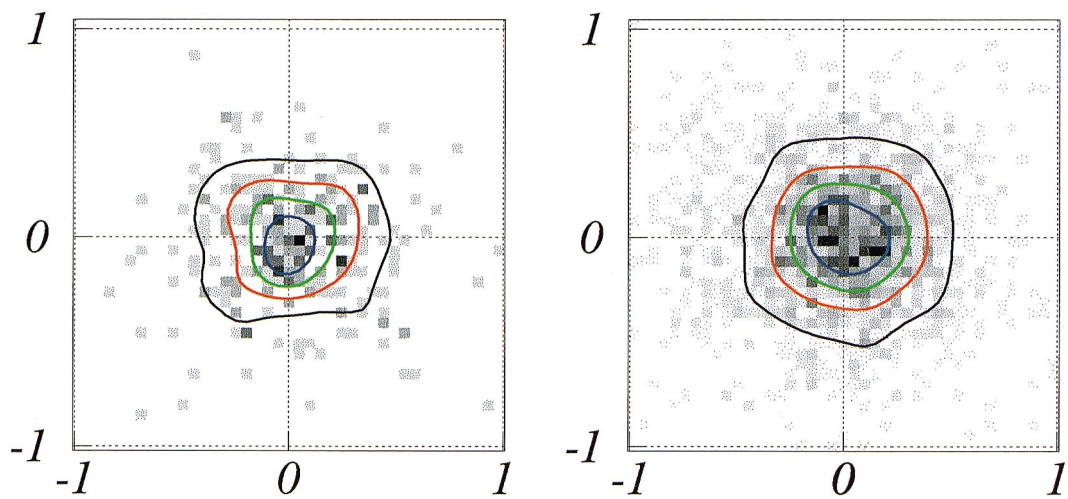


FIG. 4d

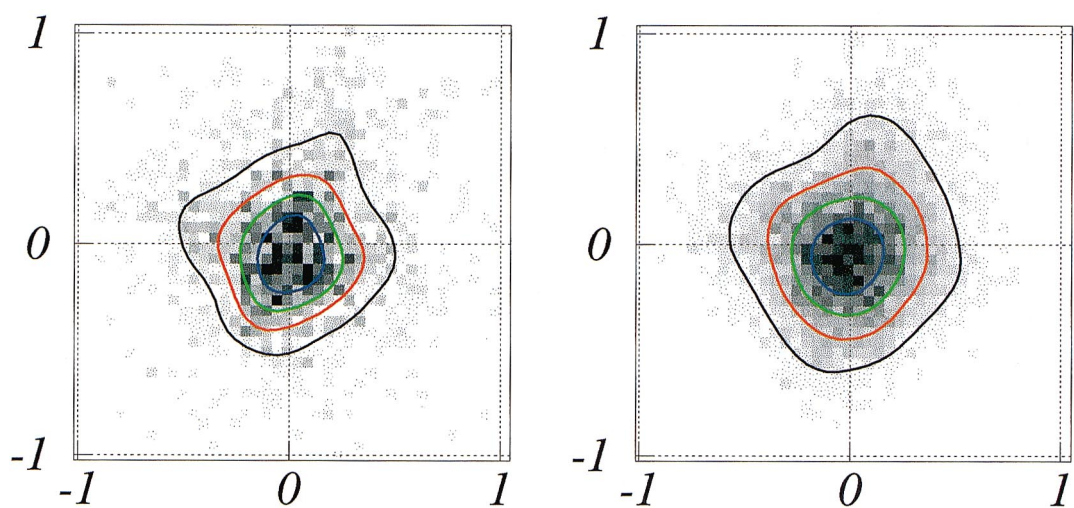


FIG. 4e

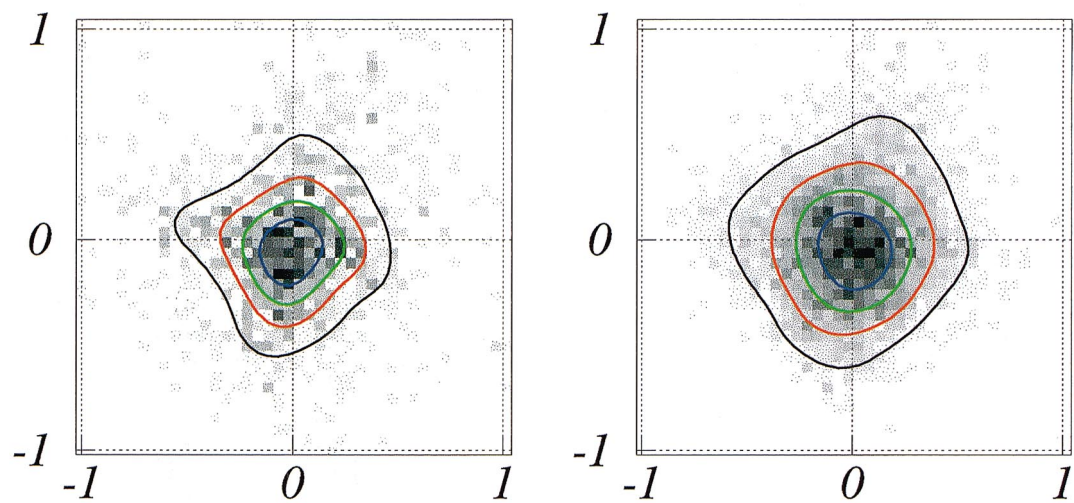


FIG. 4f

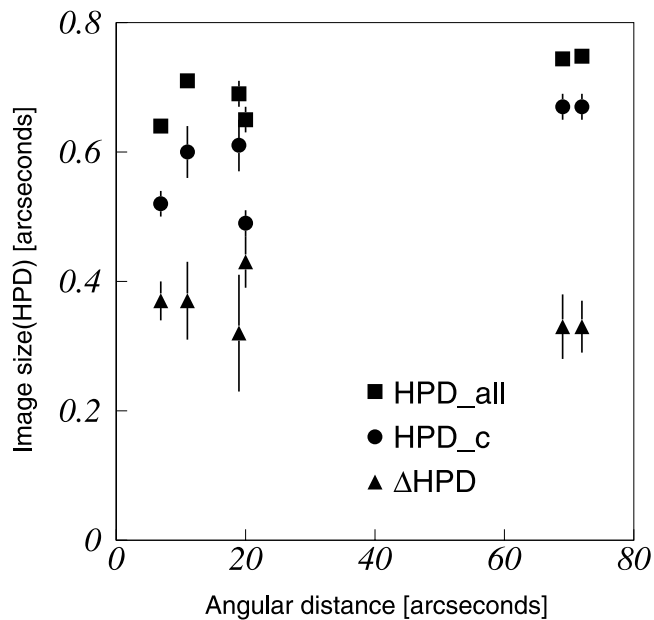


FIG. 5.—Plot of the HPD of image sizes obtained with all events and corner events as a function of the angular distance from the optical axis. Δ HPD is also plotted.

0'66 (HPD). The image degradation between the image obtained by the corner events and the image obtained by all events corresponds to that expected from the CCD pixel shape. Therefore, we can say that the image obtained using the corner events is almost free from the degradation of the image as a result of the CCD pixel shape. The corner events are generated only when X-rays enter near the pixel corner, which reduces the effective count rate. We therefore need relatively longer exposure times to obtain good statistics. Finally we should add that our method is useful only for the *Chandra* HRMA that is undersampled by the detector. Thus, for example, this technique cannot be applied to *XMM-Newton* observations.

The authors would like to express their special thanks to E. Feigelson, who kindly supplied us his *Chandra* data set, and M. W. Bautz of MIT for useful discussions. J. McDowell explained to H. T. the attitude determination system of *Chandra* in detail. This research is partially supported by ACT-JST Program, Japan Science and Technology Corporation, the Sumitomo foundation, Kurata Research Grant, the Grant-in-Aid for Scientific Research by the Ministry of Education, Culture, Sports, Science and Technology of Japan (13440062, 13874032), and by NASA contract NAS8-38252.

REFERENCES

- Burke, B. E., Gregory, J. A., Bautz, M. W., Prigozhin G. Y., Kissel, S. E., Kosicki, B. B., Loomis, A. H., & Young, D. J., 1997, *IEEE Trans*, ED-44, 1633
- Hiraga, J., Tsunemi, H., & Miyata, E. 2001, *Japanese J. Appl. Phys.*, 40, 1493
- Hiraga, J., Tsunemi, H., Yoshita, K., Miyata, E., & Ohtani, M. 1998, *Japanese J. Appl. Phys.*, 37, 4627
- Lumb, D. H., & Nousek, J. A. 1993, *Proc. SPIE*, 1736, 138
- Pivovarov, M., Jones, S., Bautz, M. W., Kissel, S., Prigozhin, G., Ricker, G., Tsunemi, H., & Miyata, E. 1998, *IEEE Trans. Nucl. Sci.*, 45, 164
- Townsley, L., Broos, P., Garmire, G., & Nousek, J. 2000, *ApJ*, 534, L139
- Tsunemi, H., Hiraga, J., Mori, K., Yoshita, K., & Miyata, E. 1999, *Nucl. Instrum. Methods Phys. Res.*, A436, 32
- Tsunemi, H., Hiraga, J., Yoshita, K., & Kitamoto, S. 1998, *Japanese J. Appl. Phys.*, 37, 2734
- Tsunemi, H., Yoshita, K., & Kitamoto, S. 1997, *Japanese J. Appl. Phys.*, 36, 2906
- Walsh, D., Carswell, R. F., & Weymann, R. J. 1979, *Nature*, 279, 381
- Yamashita, A., et al. 1997, *IEEE Trans. Nucl. Sci.* 44, 847